

Thermoelectric properties of $\text{LiCo}_{1-x}\text{M}_x\text{O}_2$ (M = Cu, Mg, Ni, Zn): Comparison with Li_yCoO_2 and Na_yCoO_2 systems

This content has been downloaded from IOPscience. Please scroll down to see the full text.

2017 Jpn. J. Appl. Phys. 56 021101

(<http://iopscience.iop.org/1347-4065/56/2/021101>)

View [the table of contents for this issue](#), or go to the [journal homepage](#) for more

Download details:

IP Address: 160.29.75.151

This content was downloaded on 05/01/2017 at 10:11

Please note that [terms and conditions apply](#).



Thermoelectric properties of $\text{LiCo}_{1-x}\text{M}_x\text{O}_2$ ($\text{M} = \text{Cu}, \text{Mg}, \text{Ni}, \text{Zn}$): Comparison with Li_yCoO_2 and Na_yCoO_2 systems

Shu Mizuno¹, Hiroyuki Fujishiro^{1*}, Mamoru Ishizawa¹, Tomoyuki Naito¹, Hirokazu Katsui², and Takashi Goto²

¹Faculty of Science and Engineering, Iwate University, Morioka 020-8551, Japan

²Institute for Materials Research, Tohoku University, Sendai 980-8577, Japan

*E-mail: fujishiro@iwate-u.ac.jp

Received June 26, 2016; accepted October 24, 2016; published online January 5, 2017

Li_yCoO_2 has a similar layered structure to Na_yCoO_2 , which is a typical p-type oxide thermoelectric material, and the average Co valence of $3 + y$ is controlled by the Li content y . We investigated the thermoelectric properties of $\text{LiCo}_{1-x}\text{M}_x\text{O}_2$ samples ($\text{M} = \text{Cu}, \text{Mg}, \text{Ni}, \text{Zn}$) for the first time at high temperatures, in which Co^{3+} was substituted by the divalent M^{2+} ions, and the average Co valence of $3 + x$ can be controlled similarly to the Li content y in Li_yCoO_2 . The substitution of the M^{2+} ions for the Co site was found to show thermoelectric properties similar to those of Li_yCoO_2 with the same average Co valence. The Mg-doped sample showed the highest thermoelectric performance at high temperatures in this study; the thermoelectric power factor P is $2.38 \times 10^{-4} \text{ W m}^{-1} \text{ K}^{-2}$ at 1173 K and the dimensionless figure of merit ZT is 0.024 at 876 K. The thermoelectric potential of $\text{LiCo}_{1-x}\text{M}_x\text{O}_2$ is discussed and compared with those of Li_yCoO_2 and Na_yCoO_2 systems. © 2017 The Japan Society of Applied Physics

1. Introduction

Thermoelectric technology that uses waste heat for power generating and cooling devices has been revived in anticipation of the forthcoming energy crisis, together with other renewable energy sources. The thermoelectric performance of materials can be evaluated from the dimensionless figure of merit ZT ($= S^2T/\rho\kappa$), and the thermoelectric power factor P ($= S^2/\rho$), where S is the Seebeck coefficient, T is the absolute temperature, ρ is the electrical resistivity, and κ is the thermal conductivity. Conventional thermoelectric bulk materials with higher ZT values include Bi_2Te_3 and PbTe , which, however, exhibit thermal and chemical instabilities in air at elevated temperatures, and contain toxic, scarce, or expensive elements.^{1–3} Nevertheless, oxide materials could be potential candidates for thermoelectric applications owing to their advantages over the heavy metallic alloys in thermal and chemical robustness values, although their potential for such applications has not yet been demonstrated. Typical p-type thermoelectric oxides are layered cobaltites such as Ti-doped $\text{Ca}_3\text{Co}_4\text{O}_9$ ($ZT = 0.3$ at 1000 K)⁴ and Na_yCoO_2 ($ZT = 0.8$ at 1050 K),⁵ in which a relatively higher Seebeck coefficient and a lower thermal conductivity are achieved owing to their layered structure. The crystal structure of Na_yCoO_2 consists of a single-atomic Na layer sandwiched between two CoO_2 layers with edge-shared CoO_6 octahedra.⁶ It is known that Na_yCoO_2 shows a wide range of Na nonstoichiometry and consists of the following three types of crystal structure depending on the Na content y : P3 type (β phase, $0.55 < y < 0.6$), P2 phase (γ phase, $0.6 < y < 0.75$), and O3 phase (α phase, $0.9 < y < 1.0$).⁷ As y decreases from one, the average valence of cobalt increases from +3 toward +4, where the concentration of magnetic Co^{4+} ions [$S = 1/2$ for low spin (LS), $S = 3/2$ for intermediate spin (IS), or $S = 5/2$ for high-spin (HS) states] increases in a nonmagnetic Co^{3+} ($S = 0$ for LS state) matrix and electronic and magnetic properties change depending on y . At about $y = 0.7$, Na_yCoO_2 exhibits an unusually large thermoelectric power and a metallic and high electrical conductivity simultaneously.^{8,9} To enhance the thermoelectric properties of Na_yCoO_2 , the Co-site substitution by 3d transition metal elements such as Cr, Mn, Fe, and Ni,^{10–12} or other elements such as Zn, B, Ti,

and Bi,^{10,13–15} and the Na-site substitution for the alkaline-earth element (Ca)¹⁶ have been widely investigated. To the best of our knowledge, the maximum ZT value of 0.68 was achieved at 965 K for the $\text{Na}_y(\text{Co}_{0.95}\text{Zn}_{0.05})\text{O}_2$ sample in polycrystals.¹⁰

Li_yCoO_2 has a layered structure similarly to Na_yCoO_2 and is the cathode material most commonly used for Li rechargeable batteries, since Li ions can be removed from and inserted into Li_yCoO_2 repeatedly through an electrochemical method.¹⁷ The electrochemical behavior and crystal structure of the Li_yCoO_2 system are well established for $0.5 \leq y \leq 1.0$,^{18,19} in which the following three types of regions exist depending on the Li content y : O3–R1 type ($0.5 < y < 0.75$), O3–R2 phase ($0.94 < y < 1.0$), and two-phase-coexistence region ($0.75 < y < 0.94$).²⁰ Li_yCoO_2 is known to exhibit a fairly large Seebeck coefficient comparable to that of Na_yCoO_2 , although the electrical resistivity is rather high.^{20,21} The thermoelectric and magnetic properties of Li_yCoO_2 have been systematically investigated at temperatures lower than 300 K for polycrystals^{22,23} and thin films.²⁴ To extend the cyclability and enhance the capacity of electrochemical Li// LiCoO_2 cells, numerous species of cations have been substituted for the Co site, such as Ni, Mn, Cr, Al, and Fe.^{25–29} The electrical conductivity and Seebeck coefficient of Mg-doped LiCoO_2 have been reported, with Mg-doped $\text{Li}_y(\text{Co}_{1-x}\text{Mg}_x)\text{O}_2$ samples showing a higher electrical conductivity than nondoped samples.³⁰ The Co site substitution by the divalent cations in LiCoO_2 introduces the magnetic Co^{4+} ions in a nonmagnetic Co^{3+} matrix, which is similar to the effect in Li_yCoO_2 obtained by the electrochemical technique. However, all the thermoelectric properties of the Li_yCoO_2 system such as $\rho(T)$ and $S(T)$ were only observed at temperatures lower than room temperature.^{23,31} There is no reported investigation of the thermoelectric properties for the $\text{Li}_y(\text{Co}_{1-x}\text{M}_x)\text{O}_2$ system at higher temperatures. In the present study, we investigated the thermoelectric properties of $\text{LiCo}_{1-x}\text{M}_x\text{O}_2$ ($\text{M} = \text{Cu}, \text{Mg}, \text{Ni}, \text{Zn}$) up to 1200 K, and compared them with those of the Li_yCoO_2 and Na_yCoO_2 systems.

2. Experimental procedure

To fabricate $\text{LiCo}_{0.8}\text{M}_{0.2}\text{O}_2$ ($\text{M} = \text{Cu}, \text{Ni}, \text{Zn}$) and LiCo_{1-x}

Mg_xO_2 ($0 \leq x \leq 0.3$) materials, Li_2CO_3 (99.9%), Co_3O_4 (99.9%), CuO (99.9%), MgO (98%), NiO (99.9%), and ZnO (99.5%) fine powders were used as raw materials. These were weighed with a stoichiometric ratio and mixed for 0.5 h using an automatic mortar in air. They were heated at 1173 K for 12 h in air and then furnace-cooled. The obtained precursor was pulverized and mixed in air for 0.5 h using an automatic mortar. The precursor powders were sintered by the SPS apparatus (NJS LABOX-110C) under a uniaxial pressure of 40–50 MPa at 1073 K for 10 min in vacuum. The obtained pellets were heat-treated at 1173 K for 2 h in air to control the oxygen stoichiometry. The relative density of the obtained pellets (10 mm in diameter and 9 mm in thickness) was about 90% of the ideal one. In this study, the Li contents in the sintered materials are supposed to be a nominal composition, assuming that the evaporation of lithium is negligibly small.

Powder X-ray diffraction (XRD) measurements were performed (Rigaku Multi Flex) at room temperature using $\text{Cu K}\alpha$ radiation to confirm the impurity phase in the sintered bulk materials. The electrical resistivity $\rho(T)$ and Seebeck coefficient $S(T)$ were simultaneously measured in the temperature range from 300 to 1200 K for a rectangular bar cut from the pellet using an automated measuring system (Ozawa Science RZ2001i), and the thermoelectric power factor $P = S^2/\rho$ was calculated. The thermal conductivity $\kappa(T)$ was measured in vacuum by a laser flash method (Ulvac-Riko TC-7000) from 300 to 873 K. The $\kappa(T)$ and $\rho(T)$ values below 300 K were also measured by a steady-state heat flow method and a four-probe method, respectively, using a laboratory-built measuring system.³²⁾ The dimensionless figure of merit, $ZT = S^2T/\rho\kappa$, was estimated using these measured values with about 20% uncertainty for each measured value.

3. Results and discussion

Figures 1(a) and 1(b) show the normalized XRD patterns of the $\text{LiCo}_{0.8}\text{M}_{0.2}\text{O}_2$ samples [$M = \text{Cu}, \text{Mg}, \text{Ni}, \text{Zn}$, and Co (nondoped)] and the magnification around the 104 peak, respectively. Although Li_yCoO_2 was reported to show a biphasic regime at $0.75 \leq y \leq 0.94$, all the diffraction peaks are readily indexed on the basis of the trigonal space group $R\bar{3}m$, and a small number of impurity phases of raw oxides with substituted elements were detected. The substitution limit of Mg for the Co site was reported to be about 5%.³⁰⁾ Each M ion seemed to substitute Co^{3+} ions up to the solubility limit, since the diffraction peak of raw oxides was detected in each sample. In Fig. 1(b), the peak angle of the 104 diffraction in the $M = \text{Cu}, \text{Zn}$ samples is the same as that in LiCoO_2 . On the other hand, that in the $M = \text{Mg}, \text{Ni}$ samples shifts toward a lower angle. The ionic radius of the Co^{3+} ion is 0.0545 nm, which is smaller than that of all the M ions: Mg^{2+} (0.072 nm), Cu^{2+} (0.073 nm), Ni^{2+} (0.069 nm), and Zn^{2+} (0.074 nm).³³⁾ These results suggest that Mg and Ni ions are easily substituted for the Co site, but the solubility limit of Cu and Zn for the Co site is still small.

Figure 2 presents the temperature dependence of the electrical resistivity $\rho(T)$, Seebeck coefficient $S(T)$, and thermoelectric power factor $P(T)$ of the $\text{LiCo}_{0.8}\text{M}_{0.2}\text{O}_2$ samples. The $\rho(T)$ of all the samples shown in Fig. 2(a) depicts a semiconducting behavior, and the absolute value of ρ changes depending on the species of the M ion. The Mg-doped

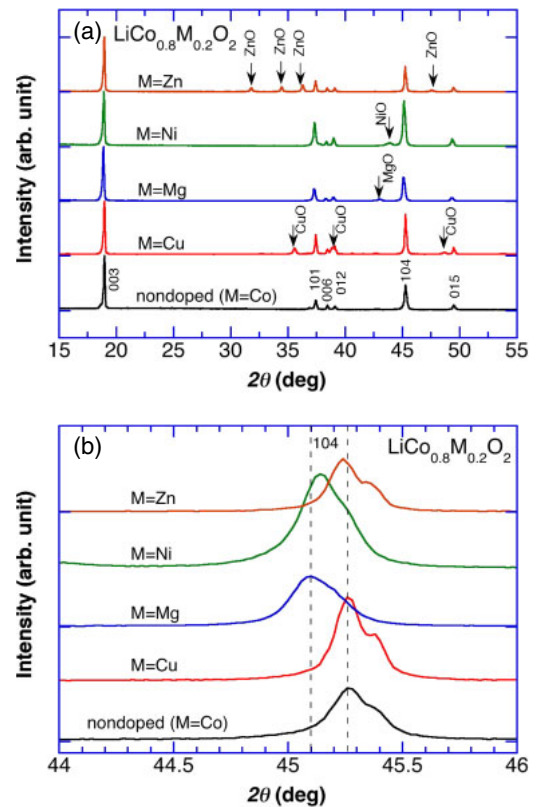


Fig. 1. (Color online) (a) XRD patterns of $\text{LiCo}_{0.8}\text{M}_{0.2}\text{O}_2$ samples [$M = \text{Cu}, \text{Mg}, \text{Ni}, \text{Zn}$, and Co (nondoped)]. (b) Enlarged XRD patterns of the 104 peak for each sample.

sample shows the lowest $\rho(T)$, which is about four orders of magnitude smaller than that of the nondoped sample at 300 K. These results are consistent with the peak shift of the XRD diffraction, as shown in Fig. 1(b), in which M ions, especially Mg^{2+} ions, substitute for the Co^{3+} site and create hole carriers.

In Fig. 2(b), the $S(T)$ value of the Mg- and Ni-doped samples is the lowest in this study. Since the Seebeck coefficient is inversely proportional to $\log n$ (n : carrier concentration) in a classical wide-gap semiconductor model, the reduced S value might be caused by the enhanced carrier concentration, and the $\rho(T)$ and $S(T)$ values are closely related to each other. However, overall, all the $S(T)$ values slightly increased with increasing T , which is inconsistent with the above relationship. The thermoelectric power factor $P(T) (= S^2/\rho)$ as shown in Fig. 2(c) increases with increasing T , and that of the Mg-doped sample is the highest with $2.38 \times 10^{-4} \text{ W m}^{-1} \text{ K}^{-2}$ at 1173 K, which results from both the lowest $\rho(T)$ and moderate $S(T)$ values. As shown in Figs. 2(a)–2(c), the reported ρ , S , and P values of $\text{Li}_{1-y}\text{CoO}_2$ at 293 K are also shown,²³⁾ in which the average Co valence is +3.25. These values are almost the same as those of the $\text{LiCo}_{0.8}\text{Mg}_{0.2}\text{O}_2$ sample with the average Co valence of +3.2. In this manner, Mg doping effectively creates positive (hole) carriers, and the Mg-doped sample shows similar thermoelectric properties to Li_yCoO_2 .

It was found that Mg doping creates hole carriers effectively and shows better thermoelectric properties, as shown in Fig. 2. To obtain optimum Mg contents, the thermoelectric properties of the $\text{LiCo}_{1-x}\text{Mg}_x\text{O}_2$ samples were investigated. Figure 3(a) shows the XRD patterns of $\text{LiCo}_{1-x}\text{Mg}_x\text{O}_2$

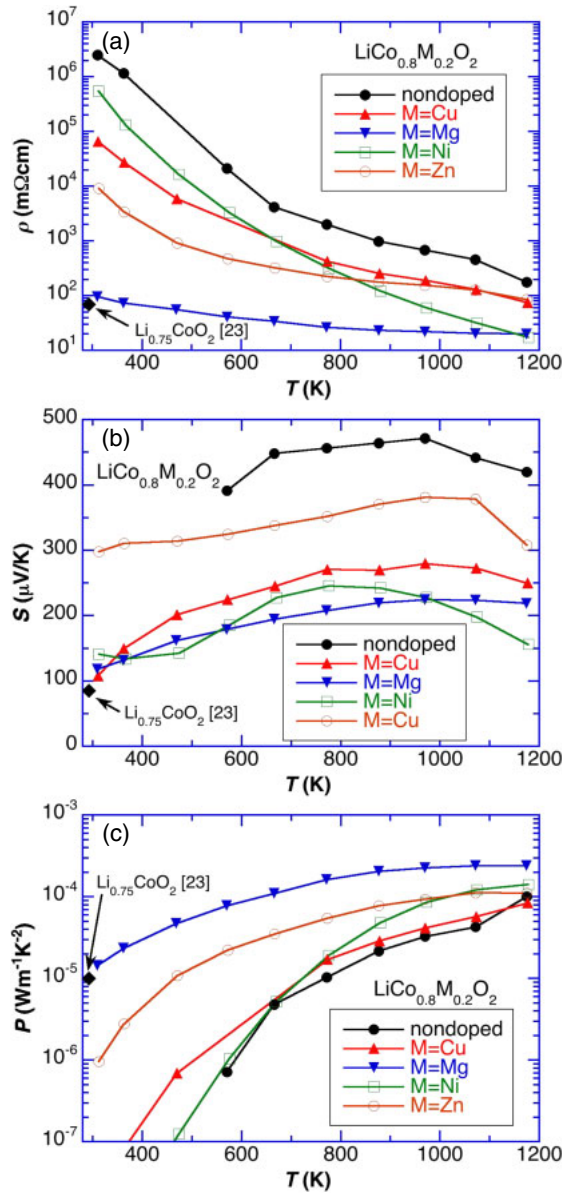


Fig. 2. (Color online) Temperature dependence of (a) electrical resistivity $\rho(T)$, (b) Seebeck coefficient $S(T)$, and (c) thermoelectric power factor $P(T)$ of $\text{LiCo}_{0.8}\text{M}_{0.2}\text{O}_2$ samples [$\text{M} = \text{Cu}, \text{Mg}, \text{Ni}, \text{Zn},$ and Co (nondoped)]. Those for the $\text{Li}_{0.75}\text{CoO}_2$ sample in Ref. 23 at 293 K are also shown.

($0 \leq x \leq 0.3$). Figure 3(b) shows the lattice constants a and c of the $\text{LiCo}_{1-x}\text{Mg}_x\text{O}_2$ samples as a function of x . The inset shows the enlarged XRD patterns near the 104 peak for each sample. For $x \leq 0.1$, the peak of the MgO raw powder was not confirmed, but for $x \geq 0.2$, the peak can be detected and increases in intensity with increasing x . In Fig. 3(b), the diffraction angle of the 104 peak decreases gradually with increasing x up to $x = 0.2$ and then tends to saturate at $x = 0.3$, which suggests that the Mg^{2+} ion substitutes for the Co^{3+} site with x and then the substitution saturates. The lattice constants of the trigonal crystal structure a and c , which were calculated using the 003 and 104 peaks, changed, depending on the Mg^{2+} substitution.

Figure 4 shows the temperature dependence of the electrical resistivity $\rho(T)$, Seebeck coefficient $S(T)$, and thermoelectric power factor $P(T)$ of $\text{LiCo}_{1-x}\text{Mg}_x\text{O}_2$ samples ($0 \leq x \leq 0.3$). The semiconducting $\rho(T)$ behavior becomes weak and the absolute ρ value decreases with increasing Mg

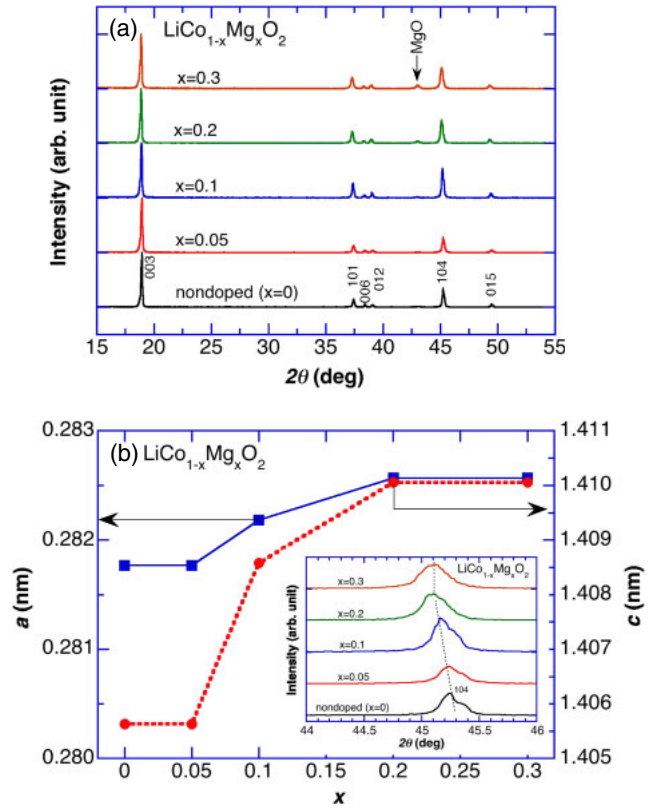


Fig. 3. (Color online) (a) XRD patterns of the $\text{LiCo}_{1-x}\text{Mg}_x\text{O}_2$ samples ($0 \leq x \leq 0.3$). (b) Lattice constants a and c of the $\text{LiCo}_{1-x}\text{Mg}_x\text{O}_2$ samples as a function of x . The inset shows the enlarged XRD patterns of the 104 peak for each sample.

content x . The absolute $S(T)$ value shown in Fig. 4(b) gradually decreases with increasing x owing to the decrease in $\rho(T)$ and then saturates. These values for the $x = 0.2$ and 0.3 samples are almost the same, which is consistent with the saturation tendency shown in Fig. 3(b). The power factor $P(T)$, which was estimated using $\rho(T)$ and $S(T)$, increases with increasing x and then also saturates for $x = 0.3$. The maximum power factor was formed to be $2.38 \times 10^{-4} \text{ W m}^{-1} \text{ K}^{-2}$ at 1173 K for the $x = 0.2$ and 0.3 samples. We calculated the P value of the $\text{LiCo}_{0.94}\text{Mg}_{0.06}\text{O}_2$ at 300 K using the reported $\rho(T)$ and $S(T)$ values,³⁰ which was smaller than that of the present sample. The difference may result from the different fabrication processes used.

In the Li_yCoO_2 system, the magnetic and related $\rho(T)$ anomalies were detected at 170 K at $y = 0.7-0.67$ and 0.5 .^{23,34,35} Mukai et al. suggested that the transition at 170 K is not magnetic but originates from either charge ordering or a change in spin state.³⁴ Figure 5 shows the $\rho(T)$ of the present $\text{LiCo}_{1-x}\text{Mg}_x\text{O}_2$ samples at $T < 300$ K. $\rho(T)$ shows a semiconducting behavior similarly to that of the samples at higher temperature. There is no anomaly in $\rho(T)$ at around 170 K for the samples. These results are in clear contrast to those of the Li_yCoO_2 system. The characteristic behaviors in the Li_yCoO_2 system are not necessarily reproduced in the $\text{LiCo}_{1-x}\text{Mg}_x\text{O}_2$ system.

Figure 6 shows the relationship between the power factor P at 300 K and the average Co valence for the present $\text{LiCo}_{1-x}\text{Mg}_x\text{O}_2$ samples ($0 \leq x \leq 0.3$). A similar relationship for the Li_yCoO_2 system at 293 K has also been shown,²³ which was calculated by us. The P value of the $\text{LiCo}_{1-x}\text{Mg}_x\text{O}_2$

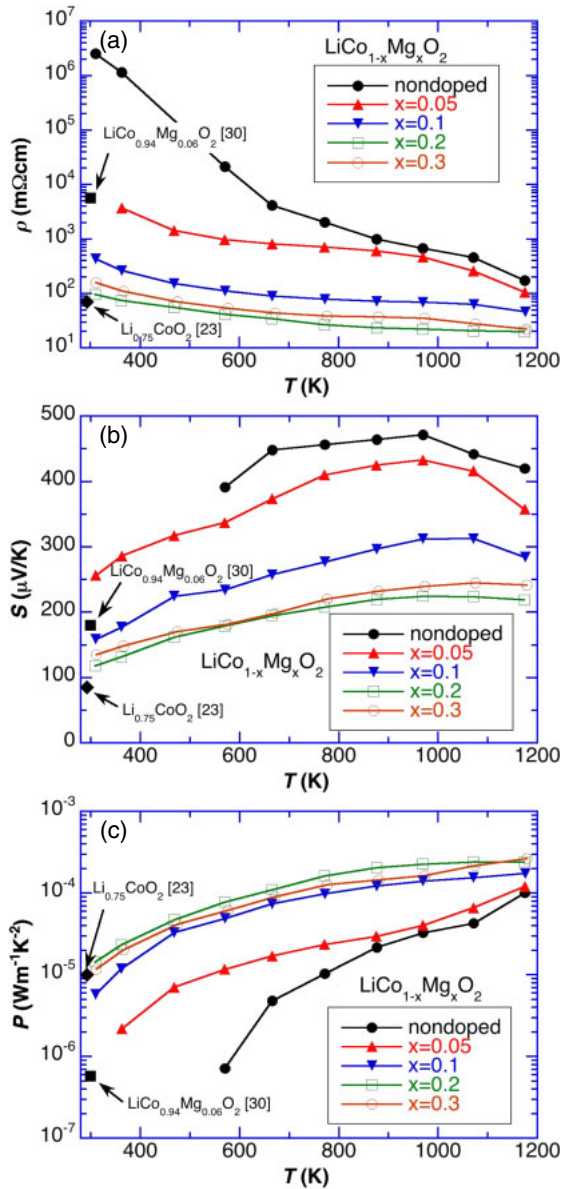


Fig. 4. (Color online) Temperature dependence of (a) electrical resistivity $\rho(T)$, (b) Seebeck coefficient $S(T)$, and (c) power factor $P(T)$ of $\text{LiCo}_{1-x}\text{Mg}_x\text{O}_2$ samples ($0 \leq x \leq 0.3$). The extracted ρ and S values, and the estimated P values from Refs. 23 and 30 are also plotted for reference.

O_2 showed a domelike dependence and reached a maximum at the Co valence of 3.2–3.3 ($x = 0.2$ – 0.3) with a continuous change, which is the same as for the Li_yCoO_2 system with a two-phase coexistence region ($0.75 < y < 0.94$). A similar relationship for the Na_yCoO_2 polycrystals is also shown in the figure,^{36,37} in which a similar dome-shaped relationship can be seen at the center of the Co valence of 3.2. However, the P value of the $\text{LiCo}_{1-x}\text{Mg}_x\text{O}_2$ system is about two orders of magnitude smaller than that of the Na_yCoO_2 system, which results from the relatively large ρ value of the $\text{LiCo}_{1-x}\text{Mg}_x\text{O}_2$ and Li_yCoO_2 systems, even though comparably large S values are achieved.

Figure 7 shows the temperature dependence of the thermal conductivity $\kappa(T)$ of the $\text{LiCo}_{0.8}\text{M}_{0.2}\text{O}_2$ samples [$M = \text{Cu}, \text{Mg}, \text{Ni}, \text{Zn},$ and Co (nondoped)] at low and high temperatures. The $\kappa(T)$ of the nondoped sample shows a large peak at a low temperature, which is in clear contrast to the reported result;³⁸ the absolute value of $\kappa(T)$ is small and $\kappa(T)$ increases

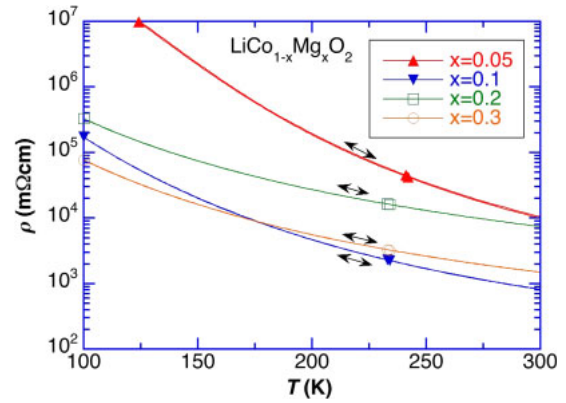


Fig. 5. (Color online) Temperature dependence of the $\rho(T)$ of the $\text{LiCo}_{1-x}\text{Mg}_x\text{O}_2$ samples ($0.05 \leq x \leq 0.3$) at $T < 300$ K.

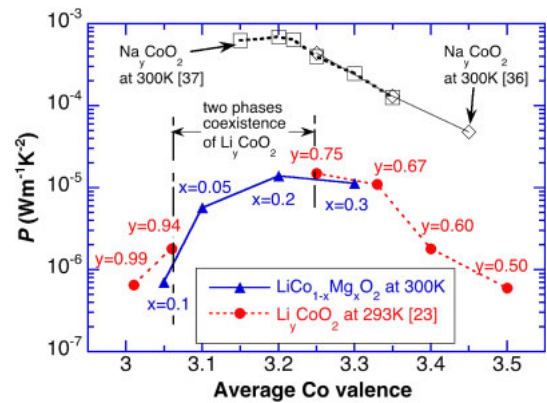


Fig. 6. (Color online) Relationship between the power factor P at 300 K and the average Co valence for the present $\text{LiCo}_{1-x}\text{Mg}_x\text{O}_2$ samples ($0 \leq x \leq 0.3$). Similar relationships for the Li_yCoO_2 system in Ref. 23 at 293 K and for the Na_yCoO_2 system (polycrystals) estimated from Refs. 36 and 37 at 300 K are also shown.

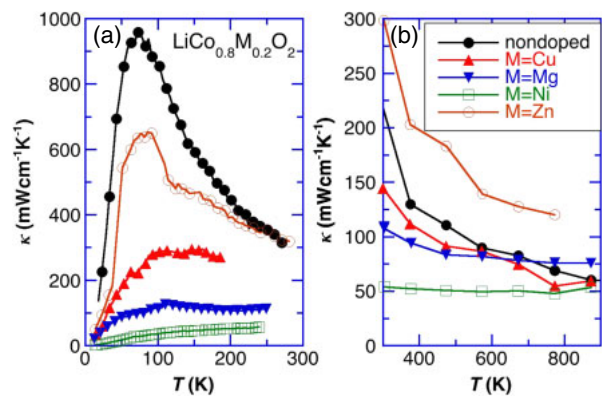


Fig. 7. (Color online) Temperature dependence of the thermal conductivity $\kappa(T)$ for the $\text{LiCo}_{0.8}\text{M}_{0.2}\text{O}_2$ samples [$M = \text{Cu}, \text{Mg}, \text{Ni}, \text{Zn},$ and Co (nondoped)] at (a) $T < 300$ K and (b) $300 < T < 900$ K.

monotonically with T . The $\kappa(T)$ peak of the $\text{LiCo}_{0.8}\text{M}_{0.2}\text{O}_2$ samples was markedly suppressed by the Co-site substitution, depending on the species of the M element; Mg and Ni doping processes effectively suppressed the $\kappa(T)$ value. These results are closely related to the solubility limit of the M element for the Co site, as shown in Figs. 1(b) and 2(a). κ is the sum of the electronic thermal conductivity κ_e and phonon thermal conductivity κ_{phonon} ($\kappa = \kappa_e + \kappa_{\text{phonon}}$). In the present samples, the

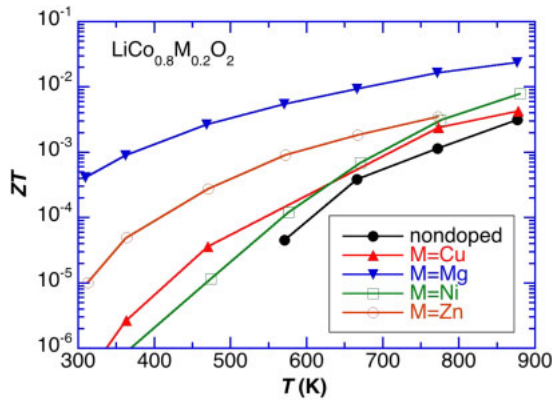


Fig. 8. (Color online) Temperature dependence of the dimensionless figure of merit $ZT(T)$ of the $\text{LiCo}_{0.8}\text{M}_{0.2}\text{O}_2$ samples [$M = \text{Cu}, \text{Mg}, \text{Ni}, \text{Zn}$, and Co (nondoped)].

thermal conduction entirely depends on phonons because the electronic contribution is negligibly small owing to the large $\rho(T)$. For example, the κ_e of the $\text{LiCo}_{0.8}\text{Mg}_{0.2}\text{O}_2$ sample is estimated to be $0.77 \text{ mW cm}^{-1} \text{ K}^{-1}$ at 800 K using Fig. 2(a) on the basis of the Wiedemann–Franz law, which is about 1% of the measured κ shown in Fig. 7(b). There have been many reports on the thermal conductivity of the Na_yCoO_2 and $\text{Na}_y(\text{Co}_{1-x}\text{M}_x)\text{O}_2$ single crystals,^{5,39,40} and polycrystals.⁴¹ However, the absolute κ values reported are fairly scattered and reliable results of the x dependence of $\kappa(T)$ have not yet been reported; the typical in-plane $\kappa(T)$ values for single crystal are $20 \text{ mW cm}^{-1} \text{ K}^{-1}$ at 300 K without a low-temperature $\kappa(T)$ peak³⁹ and $40\text{--}80 \text{ mW cm}^{-1} \text{ K}^{-1}$ at 300 K with a low-temperature $\kappa(T)$ peak.^{39,40} Since the $\kappa(T)$ value for a polycrystal is generally smaller than that for a single crystal, especially for a layered material, the $\kappa(T)$ value for Na_yCoO_2 polycrystals seems to be considerably lower than that for single crystals. In this sense, the $\kappa(T)$ of the $\text{Li}_y(\text{Co}_{1-x}\text{M}_x)\text{O}_2$ polycrystals shown in Fig. 7 is larger than that of the Na_yCoO_2 polycrystals even at higher temperatures, which is disadvantageous for a thermoelectric material from the viewpoint of $\kappa(T)$.

Figure 8 shows the temperature dependence of the dimensionless figure of merit $ZT(T)$ of the $\text{LiCo}_{0.8}\text{M}_{0.2}\text{O}_2$ samples. Among the samples, the $M = \text{Mg}$ sample shows the highest ZT value of 0.024 at 876 K, which is considerably smaller than that of the Na_yCoO_2 system, resulting from the relatively high ρ and κ values. Although Li_yCoO_2 and Na_yCoO_2 systems have similar crystal structures, a slight difference exists. Hertz et al. compared the structures of Na_yCoO_2 and Li_yCoO_2 and reported that the CoO_2 layer changes substantially with the alkali content y in the former, but is relatively constant in the latter, and that the CoO_6 octahedra in Li_yCoO_2 is less distorted.³⁵ Such a slight difference may affect the $\rho(T)$, $S(T)$, and $\kappa(T)$ values, and also the magnetic properties. The physical properties for both systems must be investigated further in detail.

4. Conclusions

The thermoelectric properties of $\text{LiCo}_{1-x}\text{M}_x\text{O}_2$ samples ($M = \text{Cu}, \text{Mg}, \text{Ni}, \text{Zn}$) have been investigated for the first time up to 1200 K and the thermoelectric potential of the $\text{LiCo}_{1-x}\text{M}_x\text{O}_2$ material has been discussed and compared with those of the Li_yCoO_2 and Na_yCoO_2 systems. The important

results and conclusions obtained from this study are summarized as follows.

1) In the $\text{LiCo}_{0.8}\text{M}_{0.2}\text{O}_2$ system, the $M = \text{Mg}$ sample displays the most effective thermoelectric properties; the thermoelectric power factor P is $2.38 \times 10^{-4} \text{ W m}^{-1} \text{ K}^{-2}$ at 1173 K and the dimensionless figure of merit ZT is 0.024 at 876 K. These values at 300 K are comparable to the reported values of $\text{Li}_{0.75}\text{CoO}_2$, suggesting that the manner of Co site substitution by Mg ions is the same as that of Co^{4+} creation to Li nonstoichiometry in the Li_yCoO_2 system.

2) In the $\text{LiCo}_{1-x}\text{Mg}_x\text{O}_2$ series ($0 \leq x \leq 0.3$), the electrical resistivity $\rho(T)$ decreases with increasing Mg contents x up to 0.2, and then saturates at $x = 0.3$. The better thermoelectric performance of the P value was achieved at $x = 0.2\text{--}0.3$ at higher temperatures.

3) The thermoelectric properties of the $\text{LiCo}_{1-x}\text{Mg}_x\text{O}_2$ series are lower than those of the Na_yCoO_2 series under an identical average Co valence because of the higher electrical resistivity $\rho(T)$ and higher thermal conductivity $\kappa(T)$ at higher temperatures.

Acknowledgment

This work was performed under the Inter-university Cooperative Research Program of the Institute for Materials Research, Tohoku University (16K0009 and 16K0203).

- 1) B. Poudel, Q. Hao, Y. Ma, Y. C. Lan, A. Minnich, B. Yu, X. Yan, D. Z. Wang, A. Muto, D. Vashaee, X. Y. Chen, J. M. Liu, M. S. Dresselhaus, G. Chen, and Z. Ren, *Science* **320**, 634 (2008).
- 2) A. D. LaLonde, Y. Z. Pei, and G. J. Snyder, *Energy Environ. Sci.* **4**, 2090 (2011).
- 3) K. F. Hsu, S. Loo, F. Guo, W. Chen, J. S. Dyck, C. Uher, T. Hogan, E. K. Polychroniadis, and M. G. Kanatzidis, *Science* **303**, 818 (2004).
- 4) L. Xu, F. Li, and Y. Wang, *J. Alloys Compd.* **501**, 115 (2010).
- 5) K. Fujita, T. Mochida, and K. Nakamura, *Jpn. J. Appl. Phys.* **40**, 4644 (2001).
- 6) C. Fouassier, G. Matejka, J.-M. Reau, and P. Hagenmuller, *J. Solid State Chem.* **6**, 532 (1973).
- 7) C. Delmas, J. Braconnier, C. Fouassier, and P. Hagenmuller, *Solid State Ionics* **3–4**, 165 (1981).
- 8) I. Terasaki, Y. Sasago, and K. Uchinokura, *Phys. Rev. B* **56**, R12685 (1997).
- 9) M. Lee, L. Viciu, L. Li, Y. Wang, M. L. Foo, S. Watauchi, R. A. Pascal, Jr., R. J. Cava, and N. P. Ong, *Nat. Mater.* **5**, 537 (2006).
- 10) M. Ito, T. Nagira, Y. Oda, S. Katsuyama, K. Majima, and H. Nagai, *Mater. Trans.* **43**, 601 (2002).
- 11) M. Ito and T. Nagira, *Mater. Trans.* **46**, 1456 (2005).
- 12) L. Wang, M. Wang, and D. Zhao, *J. Alloys Compd.* **471**, 519 (2009).
- 13) E. Altin, E. Oz, S. Demirel, and A. Bayri, *Appl. Phys. A* **119**, 1187 (2015).
- 14) A. Klyndyuk, N. Krasutskaya, L. Evseeva, E. Chizhova, and S. Tanaeva, *Univ. J. Mater. Sci.* **3**, 27 (2015).
- 15) Z. Tian, X. Wang, J. Liu, Z. Lin, Y. Hu, Y. Wu, C. Han, and Z. Hu, *J. Alloys Compd.* **661**, 161 (2016).
- 16) E. Ermawan and S. Poertadji, *Int. J. Eng. Technol.* **15**, 42 (2015).
- 17) K. Nakamura, H. Ohno, K. Okamura, Y. Michihiro, T. Moriga, I. Nakabayashi, and T. Kanashiro, *Solid State Ionics* **177**, 821 (2006).
- 18) N. Reimers and J. R. Dalm, *J. Electrochem. Soc.* **139**, 2091 (1992).
- 19) T. Ohzuku and A. Ueda, *J. Electrochem. Soc.* **141**, 2972 (1994).
- 20) M. Ménétrier, I. Saadoune, S. Levasseur, and C. Delmas, *J. Mater. Chem.* **9**, 1135 (1999).
- 21) J. Molenda, A. Stoklosa, and T. Bak, *Solid State Ionics* **36**, 53 (1989).
- 22) T. Motohashi, T. Ono, Y. Sugimoto, S. Kikkawa, R. Kanno, M. Karppinen, and H. Yamauchi, *Phys. Rev. B* **80**, 165114 (2009).
- 23) T. Motohashi, Y. Sugimoto, T. Sasagawa, W. Koshibae, T. Tohyama, and S. Kikkawa, *Phys. Rev. B* **83**, 195128 (2011).
- 24) Y. Ishida, A. Mizutani, K. Sugiura, H. Ohta, and K. Koumoto, *Phys. Rev. B* **82**, 075325 (2010).
- 25) C. Delmas, I. Saadoune, and A. Rougier, *J. Power Sources* **44**, 595 (1993).

- 26) R. Stoyanova, E. Zhecheva, and L. Zarkova, *Solid State Ionics* **73**, 233 (1994).
- 27) C. D. W. Jones, E. Rossen, and J. R. Dahn, *Solid State Ionics* **68**, 65 (1994).
- 28) Y. I. Yang, B. Huang, H. Wang, G. R. Maskaly, G. Ceder, D. R. Sadoway, Y. M. Chiang, H. Liu, and H. Tamura, *J. Power Sources* **81–82**, 589 (1999).
- 29) H. Kobayashi, H. Shigemura, M. Tabuchi, H. Sakaebe, K. Ado, H. Kageyama, A. Hirano, R. Kanno, M. Wakita, S. Morimoto, and S. Nasu, *J. Electrochem. Soc.* **147**, 960 (2000).
- 30) S. Levasseur, M. Menetrier, and C. Delmas, *Chem. Mater.* **14**, 3584 (2002).
- 31) D. Carlier, M. Menetrier, and C. Delmas, *J. Mater. Chem.* **11**, 594 (2001).
- 32) H. Fujishiro, M. Ikebe, T. Naito, K. Noto, S. Kobayashi, and S. Yoshizawa, *Jpn. J. Appl. Phys.* **33**, 4965 (1994).
- 33) R. D. Shannon, *Acta Crystallogr., Sect. A* **32**, 751 (1976).
- 34) K. Mukai, Y. Ikedo, H. Nozaki, J. Sugiyama, K. Nishiyama, D. Andreica, A. Amado, P. L. Russo, E. J. Ansaldo, J. H. Brewer, K. H. Chow, K. Ariyoshi, and T. Ohzuku, *Phys. Rev. Lett.* **99**, 087601 (2007).
- 35) J. T. Hertz, Q. Huang, T. McQueen, T. Klimczuk, J. W. G. Bos, L. Viciu, and R. J. Cava, *Phys. Rev. B* **77**, 075119 (2008).
- 36) T. Motohashi, E. Naujalis, R. Ueda, K. Iwasa, M. Karppinen, and H. Yamauchi, *Appl. Phys. Lett.* **79**, 1480 (2001).
- 37) P. Liu, G. Chen, Y. Cui, H. Zhang, F. Xiao, L. Wang, and H. Nakano, *Solid State Ionics* **179**, 2308 (2008).
- 38) K. Takahata and I. Terasaki, *Jpn. J. Appl. Phys.* **41**, 763 (2002).
- 39) X. Tang and T. M. Tritt, *J. South Carolina Acad. Sci.* **6**, 10 (2008).
- 40) A. Satake, H. Tanaka, T. Ohkawa, T. Fujii, and I. Terasaki, *J. Appl. Phys.* **96**, 931 (2004).
- 41) K. Takahata, Y. Iguchi, D. Tanaka, T. Itoh, and I. Terasaki, *Phys. Rev. B* **61**, 12551 (2000).